# Onset and Stability of Convection in Porous Media: Visualization by Magnetic Resonance Imaging

M. D. Shattuck and R. P. Behringer
*Department of Physics and Center for Nonlinear and Complex Systems, Duke University, Durham, North Carolina 27708-0305*

G. A. Johnson
*Center for In-Vivo Microscopy, Duke University Medical Center, Durham, North Carolina 27710*

J. G. Georgiadis
*Mechanical and Industrial Engineering Department, University of Illinois, Urbana-Champaign, Urbana, Illinois 61801*
(Received 8 July 1994)

Using magnetic resonance imaging, we examine the onset and stability of porous media convection (PMC) in packings of solid spheres. Nominally, PMC resembles Rayleigh-Bénard convection, except that there should be no vertical vorticity. We find pinned defects in convection patterns for disordered sphere packings. Roll-like structures form in regularly packed media, with rapid relaxation to stable patterns within the expected stable range. The size of up flow regions decreases relative to down flow regions with increasing Rayleigh number, producing a novel time dependent state for $\mathrm{Ra}/\mathrm{Ra}_c > 6$.

PACS numbers: 44.30.+v, 47.20.Bp, 47.54.+r

Nonlinear pattern forming systems have been the subject of considerable recent interest [1]. An intensively studied example [2] is Rayleigh-Bénard convection (RBC): a thin horizontal layer of fluid is heated from below creating a temperature difference $\Delta T$ across a layer of height $d$. Buoyancy overcomes dissipation at $\Delta T = \Delta T_c$, corresponding to a critical value $\mathrm{Ra}_c$ of the Rayleigh number Ra.

An analogous form of convection, porous media convection (PMC), or Horton-Rodgers-Lapwood convection [3], can occur for a fluid-saturated matrix [4]. In the laboratory, the matrix is often a packing of spherical particles, but many other matrix geometries are possible [5]. PMC belongs to a class of flows which have substantial technical relevance [6], and it is interesting as a nonlinear pattern forming system.

PMC has a number of features in common with RBC. PMC is expected to occur via a forward pitchfork bifurcation at a critical Rayleigh number to a flow consisting of rolls with a well-defined wave number $q = q_c(= \pi)$. Within a well-defined region in Ra-$q$ space, straight parallel PMC rolls are expected to be stable and outside that region to be subject to instabilities [7,8] that have parallels in RBC.

Several features distinguish PMC from RBC. Flows in porous media are typically described by Darcy's law, this is intended to represent the average properties of the flow on a scale which is large compared to the pore size. By contrast, RBC is described by the Navier-Stokes equations. Spatial variations in the matrix can lead to variations in Ra which are usually absent in RBC. These variations can lead to anisotropy and to localized regions of enhanced convection [9]. Consequently, this system has a novel feature which clearly distinguishes it from RBC and introduces the possibility of new kinds of dynamics [10].

The solid matrix also makes visualization of the flow very difficult. Until recently [5], experiments [11,12] either did not effectively achieve visualization or achieved it at the price of large perturbations to the system. To our knowledge, this work presents the first nonperturbative, quantitative, imaging of the horizontal convection pattern in a conventional PMC experiment consisting of packed spheres and the only velocity determination, regardless of the solid matrix. We use magnetic resonance imaging (MRI) [13], which permits the visualization of the local density, velocity, and temperature of a fluid consisting of molecules with unpaired nuclear spins, such as water. Here we present results for the local velocity of the flow.

The dynamics of PMC for homogeneous isotropic media are typically described [14] by Darcy's law (with an acceleration term), by a heat equation, and by an equation of continuity. The first of these is

$$(\rho/\phi)\partial \mathbf{v}\partial t = -B[\nabla P + (\eta/\gamma)\mathbf{v}] + p\mathbf{g}. \quad (1)$$

Here $B$ is a dimensionless acceleration coefficient, assumed to be $\sim 1$, $\gamma$ is the medium permeability, $\phi$ is the porosity, and $\rho$ and $\eta$ are the fluid density and viscosity, respectively. In the usual Boussinesq approximation, $\rho$ in the term $\rho\mathbf{g}$ is assumed to be a linear function of temperature. For a random packing of spheres [15] of diameter $\delta$, $\gamma$ is typically represented by $\gamma = \delta^2\phi^3/150(1-\phi)^2$.

In dimensionless form, these equations contain two parameters: the Prandtl number

$$\mathrm{Pr} = \nu/\kappa \quad (2)$$

and the porous Rayleigh number

$$\mathrm{Ra} = \alpha g d \gamma \Delta T/\nu\kappa. \quad (3)$$

 0031-9007/95/75(10)/1934(4)$06.00 

Here $\alpha$ and $\nu$ are, respectively, the fluid isobaric thermal expansion coefficient and kinematic viscosity. $\kappa$ is an effective thermal diffusivity with contributions from the fluid and matrix. The porous Rayleigh number differs from the RBC counterpart by a factor of the Darcy number $\mathrm{Da} = \gamma/d^2$. If the solid matrix is not isotropic, terms involving $\gamma$ and $\kappa$ must be replaced by tensor expressions [8], $q_c \neq \pi$, and the region of stable convective states in the Ra-$q$ plane typically changes [7].

The $z$ component of the curl of Eq. (1) yields the dynamics of the vertical vorticity $\Omega_z$:

$$\partial\Omega_z/\partial t = -(B\nu\phi/\gamma)\Omega_z . \quad (4)$$

$\Omega_z$ decays exponentially, independently of the other dynamics, with a time constant $\tau_{\Omega_z} = \gamma/B\nu\phi = (\mathrm{Da}/B\mathrm{Pr}\phi)d^2/\kappa$. Typically (i.e., water with $\delta = 1$ mm), $\tau_{\Omega_z} \simeq 5$ ms. The next fastest time in the system is the vertical thermal diffusion time $\tau_v = d^2/\kappa$, which is typically $\sim 10^2$ to $10^3$ s (1560 s for these experiments). The Darcy description implies no vertical vorticity after the rapid decay of any initial transients. By contrast, vertical vorticity occurs in RBC and is related to the complex dynamics observed for low to moderate Pr fluids [16–18]. Because $\Omega_z = 0$ is predicted for Darcian convection, we might expect that such states would be absent for this system.

The Darcy description assumes that the pore scale satisfies $\delta \ll d$, i.e., $\mathrm{Da} \ll 1$. But, in experiments, $\delta$ cannot be made very small without requiring very large temperature differences, since $\Delta T \propto \mathrm{Ra}/\gamma \propto \delta^{-2}$. And if $d$ is made large, for instance $d \gg 1$ cm, then the thermal relaxation times become prohibitively large. In reality, only the condition $\delta < d$ can be met. For instance, an order of magnitude decrease in $\delta/d$ would require either an unacceptible increase of the onset $\Delta T$ by 2 orders of magnitude or a correspondingly large increase in the relaxation times. Although other changes in $d$ and/or $\delta$ are possible, *experiments in general* on porous convection for sphere packings (or similar structures) and typical fluids cannot operate in the limit $\delta/d \rightarrow 0$. Consequently, Darcy's law, Eq. (1), may need to be modified. We are unaware of rigorous substitute models for Darcy's law under these circumstances, but one possibility may be to allow the parameters, such as $\gamma$, to be functions of space. In that event, Eq. (4) no longer applies, and interesting new dynamics are possible [9,10]. Some experimental information concerning $\delta/d$ does exist. Close, Symmons, and White [11] find that critical Rayleigh numbers are not strongly affected by small $\delta/d$ even when this quantity is $\sim 2$. However, experimental tests of pattern selection are lacking, and the applicability of the Darcy formalism has generally been unverified. The present experiments indicate which predictions of the Darcy formalism are actually manifested in experiment.

The experiments are carried out using a specially designed cell (see inset, Fig. 3) for use in an MRI environment that does not allow the use of electrically conditioning materials or media with large variations of magnetic susceptibility. The porous medium consists of monodisperse plastic beads of diameter 3.2 mm sandwiched between two aluminum nitride (AlN) plates. The fluid is pure water. AlN is an electrical insulator but has high thermal conductivity, about $\frac{1}{3}$ that of copper. Temperatures on either side of the layer are maintained to better than 5 mK (compared to $\Delta T_c \simeq 10$ K) by independent circulating water baths. The sidewalls are made of Delrin. The cell can be easily inserted into a horizontal-bore 2 T MRI magnet. A computer controls the experiment and carries out a sequence of temperature steps and MRI scans. Details of the MRI technique are given elsewhere [19]. We have obtained heat transport data for some runs by replacing one of the AlN plates by a thin sandwich consisting of a sheet of plastic between two sheets of AlN. The temperature drop across the thin sheet, as well as the temperature drop across the fluid-saturated matrix, yields the heat transport, and hence the Nusselt number $N$ defined as the heat flux across the fluid normalized by the conductive heat flux. $N = 1$ for $\mathrm{Ra} < \mathrm{Ra}_c$ and $N$ grows as the convective strength increases.

We consider first results for a cell with cylindrical side walls and a disordered packing obtained by pouring spheres into the convection layer. The aspect ratio $\Gamma = \mathrm{radius}/d = 5.00$. In fact, this packing has short-range order consisting of spatially ordered regions which are smaller than the cell, separated by defects in the packing pattern such as grain boundaries. A typical image showing the vertically averaged vertical velocity is given in Fig. 1. Bright patterns corresponds to upflow and dark to down flow. The convection patterns consist of disordered roll-like structures. Convection begins first in regions where there are packing defects because they tend

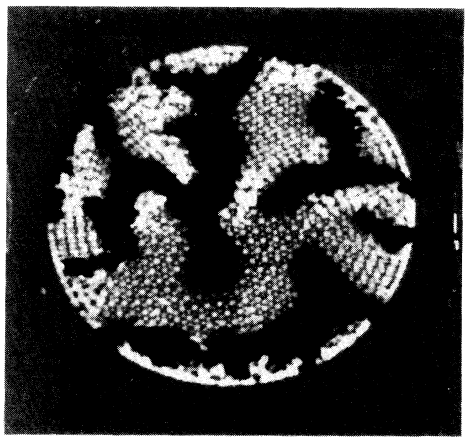

FIG. 1. MRI velocity images of convection in a cylindrical container of aspect ratio $\mathrm{radius}/d = 5.00$. The packing is disordered. These images give the vertical velocity averaged over the thickness of the layer. Upflows are lighter and downflows are darker.

to increase the local permeability. This is in qualitative agreement with the calculations of Zimmermann, Seesselberg, and Petruccione [9] who considered random variations of Ra on the Swift-Hohenberg model. Even at higher Ra, where convection is fully developed throughout the container, the packing defects often remain as pinning sites of the convection pattern. The roll patterns differ qualitatively from those seen in RBC since rolls are not necessarily forced to be normal to the side walls.

We next consider convection in a layer with a hexagonal planform. This geometry was chosen because it is defect-free within the interior, and it allows a sphere packing that is identical at all the side walls. Within each layer, the beads are close packed in a regular triangular pattern. Four layers of beads are stacked in a vertical packing order *ABCA* to form a matrix with an aspect ratio $\Gamma = L/d = 9.05$, where $L$ is the greatest distance between points of the hexagon. This packing is essentially free of defects except at the edges, where there is a periodic variation of the local properties. Figures 2(b)–(f) show typical steady convection patterns obtained for this cell. For Figs. 2(b) and 2(c) $\mathrm{Ra}/\mathrm{Ra}_c = 3.0$; Figs. 2(d)–2(f) are representative patterns found on recycling through onset, all at $\mathrm{Ra}/\mathrm{Ra}_c = 2.0$. Figure 2(a) shows a pattern at $\mathrm{Ra}/\mathrm{Ra}_c = 8.0$ where time dependence has set in. Approximately parallel rolls fill the cell. However, the rolls may curve and need not be of uniform width; rolls can pinch or terminate within the interior of the cell. As with the previous container, convection occurs first in regions of locally high porosity, in this case along the sidewall. The convection near the walls consists of a nearly regular array of very narrow rolls having a significantly larger $q$ than the primary pattern. The well rolls appear to have only a limited influence over the forcing of the main pattern.

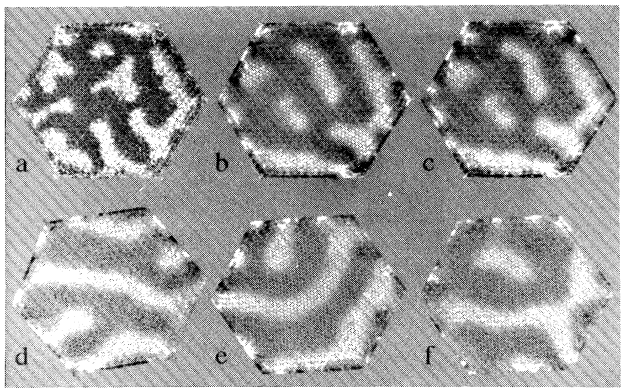


FIG. 2. MRI velocity images for a hexagonal cell. (a) A typical time-dependent state at $\mathrm{Ra}/\mathrm{Ra}_c = 8.0$ (b),(c) Relaxation following a quench from $\mathrm{Ra}/\mathrm{Ra}_c = 8.0$ of part (a) to $\mathrm{Ra}/\mathrm{Ra}_c = 3.0$. Part (b) was acquired $2\tau_v$ after the quench was made; part (c) was acquired $100\tau_v$ later and is almost identical to (b). (d)–(f) Representative steady convection patterns all for $\mathrm{Ra}/\mathrm{Ra}_c = 2.0$. Each of (d)–(f) corresponds to a different cycling through the onset of convection.

The Nusselt number for the hexagonal sidewalls is given in Fig. 3. This quantity shows a relatively sharp transition to convection. The arrows to the right and left show, respectively, where the side rolls are first detected and where convection can first be discerned in the interior. The slope $S \equiv \mathrm{Ra}_c dN/dR = 0.73$ is smaller than the predicted value [8] $S = 2$ for homogeneous isotropic media but in accord with other experients of comparable $\delta/d$ [11].

For isotropic porous media, the dimensionless wave vector of the rolls is predicted to be $\pi$, corresponding to rolls of width $d$. The rolls are clearly somewhat larger than $d$, and we estimate $q \simeq 0.7\pi$ over a large range of Ra. Also, the width of the upflow rolls, $\lambda_{\mathrm{up}}$, differs from that for the downflow rolls, $\lambda_{\mathrm{down}}$, except near onset. The ratio $\lambda_{\mathrm{up}}/\lambda_{\mathrm{down}}$ decreases with Ra, as shown in Fig. 4.

We turn now to the time evolution of the patterns. Above $\mathrm{Ra}/\mathrm{Ra}_c \simeq 6$, the patterns evolve continuously with time. Small regions of intense upflow wander inside a large sea of weaker downflow [Fig. 2(a), for $\mathrm{Ra}/\mathrm{Ra}_c = 8.0$] over times of at least several days, i.e., for as long as we have observed them. These times are of order of the horizontal diffusion time $L^2/\kappa$. This state does not obviously resemble predicted wave shapes [7,8] for the instabilities that destabilize parallel rolls (i.e., oscillatory, cross roll or skew varicose instabilities).

If Ra is quenched rapidly from $\sim 8\mathrm{Ra}_c$ to $\mathrm{Ra} = 3.0\mathrm{Ra}_c$, relaxation of the pattern to a steady state is obtained in a relatively short time, as seen in the time sequence of Figs. 2(a)–(c). Part (a) shows the time-

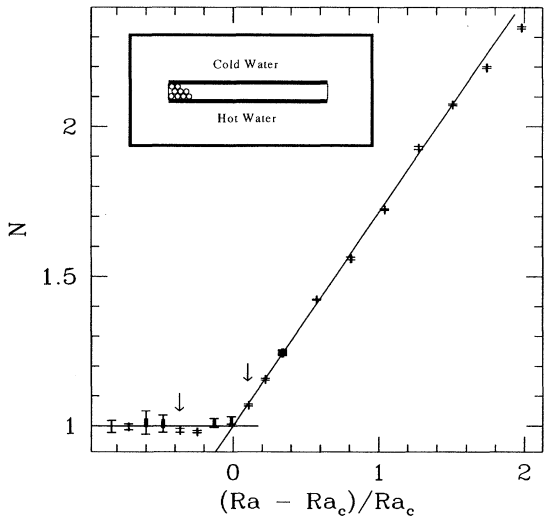


FIG. 3. Nusselt number vs $(\mathrm{Ra} - \mathrm{Ra}_c)/\mathrm{Ra}_c$ for the hexagonal cell. The arrow to the left indicates when narrow convection rolls first form along the side walls. The arrow to the right indicates when the MRI first detects convection in the interior of the cell. Inset: Schematic of the convection cell used in the MRI apparatus. The convection layer is indicated by small circles.

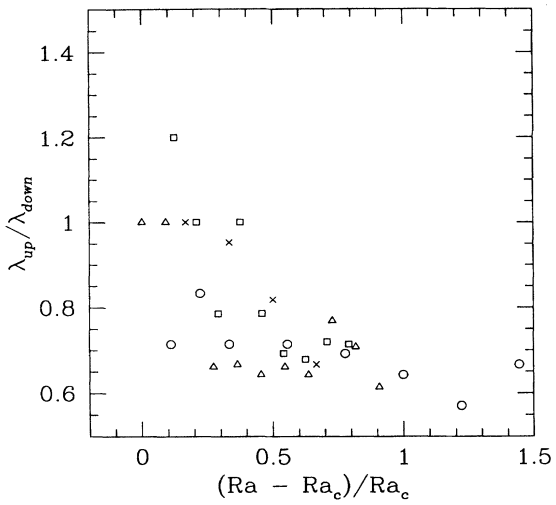


FIG. 4. Ratio of the upflow roll width $\lambda_{up}$ to the downflow roll width $\lambda_{down}$ vs $(Ra - Ra_c)/R_c$. The various symbols represent four different experimental runs.

dependent state at $Ra/Ra_c = 8.0$, just before the quench; part (b) shows the state at $Ra/Ra_c = 3.0$ about $2\tau_v$ after the quench; part (c) shows the pattern is then virtually unchanged after waiting $100\tau_v$ longer. Quenches of this type [20] are useful because they test for the existence of time-dependent states in the regime in which only steady states are expected but whose basins of attraction may not be encountered if Ra is ramped slowly. Similar quenches ending at $Ra/Ra_c = 2.0, 4.0$, and 6.0 produce rapid relaxation to patterns which are steady, except possibly near the boundary, for times up to several days. We conclude that there is a substantial range in Ra characterized by rapid relaxation to steady-state flows. This is consistent with the expectations discussed above, assuming that Darcy's law applies.

We conclude with the following points. The present experiments have shown that steady convective states in a porous medium consisting of packed spheres exist for moderate $\Gamma$ and a range of Ra, which is consistent with predictions. Approximately parallel roll states are obtained only when the packing is regular; otherwise, defects produce pinning and irregular patterns. There are several observations that cannot be explained in the context of existing theory. These include the lower-than-expected wave vector, the broken symmetry of up- and downflows, and the time-dependent states obtained at large Ra. In all of these effects, the structure of the sphere packing presumably plays a important and largely unexplored role. In particular, there is little theory to address the experimentally relevant regime in which the pore scale is not microscopically small.

This work was supported by the U.S. DOE, Office of Basic Energy Sciences, Grant No. DEFG05-90R14141 and (G. A. J.) by NIH Grant No. P41 RR05959 and NSF Grant No. CDR-8622201.

[1] M. C. Cross and P. C. Hohenberg, Rev. Mod. Phys. **65**, 851 (1993).
[2] R. P. Behringer, Rev. Mod. Phys. **57**, 657 (1985).
[3] C. W. Horton and R. T. Rodgers, J. Appl. Phys. **16**, 367 (1945); E. Lapwood, Proc. Cambridge Philos. Soc. **44**, 508 (1948).
[4] M. A. Combernous and S. A. Bories, Hydroscience **10**, 231 (1975).
[5] Laurens Howle, R. P. Behringer, and John Georgiadis, Nature (London) **362**, 230 (1993).
[6] J. G. Georgiadis, in *Convective Heat and Mass Transfer in Porous Media,* edited by S. Kakac, B. Kilkis, F. A. Kulacki, and F. Arinc, NATO Advanced Study Institute Series Vol. E 196 (Kluwer Academic Publishers, Dordrecht, The Netherlands, 1991) pp. 1073–1088.
[7] J. M. Strauss, J. Fluid Mech. **64**, 51 (1974); J. M. Strauss and G. Schubert, J. Fluid Mech. **87**, 385 (1978).
[8] O. Kvernvold and P. Tyvand, J. Fluid Mech. **90**, 609 (1979); **99**, 673 (1980).
[9] Walter Zimmermann, Markus Seesselberg, and Francesco Petruccione, Phys. Rev. E **48**, 2699 (1993).
[10] E. Knobloch, J. Hettel, and G. Dangelmayr, Phys. Rev. Lett. **74**, 4839 (1995).
[11] D. J. Close, J. G. Symmons, and R. F. White, Int. J. Heat Mass Transfer **28**, 2371 (1985).
[12] J. W. Elder, J. Fluid Mech. **27**, 29 (1967); T. Kaneko, M. Mohtade, and K. Aziz, Int. J. Heat Mass Transfer **17**, 485 (1974); C. R. B. Lister, J. Fluid Mech. **214**, 287 (1990); B. T. Murray and C. F. Chen, J. Fluid Mech. **201**, 147 (1989).
[13] Paul T. Callaghan, *Principles of Nuclear Magnetic Resonance Microscopy* (Clarendon Press, Oxford, 1991); P. R. Moran,Magn. Reson. Imaging, **1**, 197 (1982).
[14] Jacob Bear, *Dynamics of Fluids in Porous Media* (Dover, New York, 1988); D. A. Nield and A. Bejan, *Convection in Porous Media* (Springer, New York, 1992).
[15] S. Ergun, Chem. Eng. Prog. **48**, 89 (1952).
[16] E. D. Siggia and A. Zippelius, Phys. Rev. Lett. **47**, 835 (1981).
[17] M. C. Cross and A. C. Newell, Physica (Amsterdam) **10D**, 299 (1984).
[18] Stephen W. Morris, Eberhard Bobenschatz, David S. Cannell, and Guenter Ahlers, Phys. Rev. Lett. **71**, 2026 (1993).
[19] J. Georgiadis, R. Behringer, M. Shattuck, and G. A. Johnson, in Proceedings of the 9th Symposium on Energy Sciences, 1991 (to be published).
[20] Guenter Ahlers, David S. Cannell, and V. Steinberg, Phys. Rev. Lett. **54**, 1373 (1985); M. S. Heutmaker, P. N. Fraenkel, and J. P. Gollub, Phys. Rev. Lett. **54**, 1369 (1985).

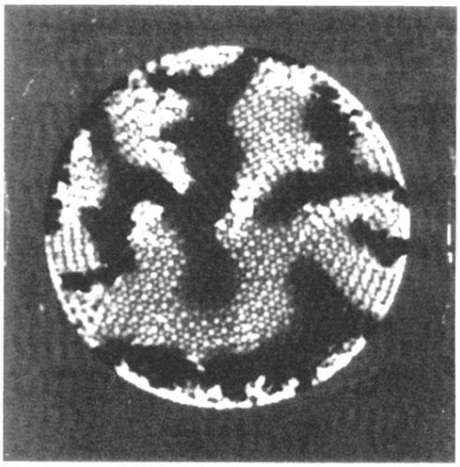

FIG. 1. MRI velocity images of convection in a cylindrical container of aspect ratio radius/$d$ = 5.00. The packing is disordered. These images give the vertical velocity averaged over the thickness of the layer. Upflows are lighter and downflows are darker.

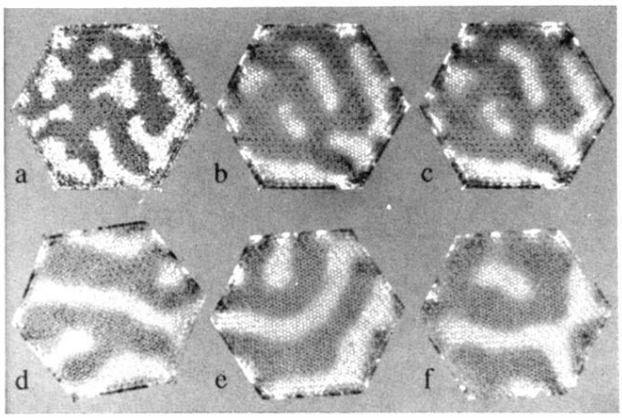


FIG. 2. MRI velocity images for a hexagonal cell. (a) A typical time-dependent state at $\mathrm{Ra}/\mathrm{Ra}_c = 8.0$ (b),(c) Relaxation following a quench from $\mathrm{Ra}/\mathrm{Ra}_c = 8.0$ of part (a) to $\mathrm{Ra}/\mathrm{Ra}_c = 3.0$. Part (b) was acquired $2\tau_v$ after the quench was made; part (c) was acquired $100\tau_v$ later and is almost identical to (b). (d)–(f) Representative steady convection patterns all for $\mathrm{Ra}/\mathrm{Ra}_c = 2.0$. Each of (d)–(f) corresponds to a different cycling through the onset of convection.